

Software Solution for Digital-Reflectometry of the Surface Structure of the Metal-Oxide Corrode Films

Oleksandr O. Matiushkin¹, Roman D. Yershov¹, Volodymyr P. Voytenko¹, Aleksandr A. Korolev²

¹Industrial Electronics Department, ²Food Technologies Department
Chernihiv National University of Technology (CNUT)
Chernihiv, Ukraine

e-mail: matushkin1994@gmail.com; roman.d.yershov@gmail.com

Abstract—The problems of measurement the thickness of metal-oxide corrode film by using of customer-grade digital scanner and camera are considered. The theoretical background of dependence between color components, reflected wavelengths, and oxide film thickness for given metal alloy is described. Based on it the problem of violet color wavelength interpretation is partially solved. Object-oriented platform-independent software solution written on C++ is implemented and verified by existing experimental results.

Keywords—*thin film, corrode, rust, oxide, colour wavelength, reflectometry, data processing software*

INTRODUCTION

The surface structure and its profile thickness of oxide layer thin films, whose are formed around metals and alloys under the influence of humidity, gases and temperature, can be obtained by using of reflectometry [1]. The quality and numeric analysis of layer properties in nano-scale resolution is impossible without precision data acquisition sensors and high-productive computers, whose are equipped with various algorithms [2]. For this purposes a customer high-resolution scanner [5] or video microprobe [3] also can be used.

A phase-modulation attachment to hand-operated ellipsometers [4] allow to keep accuracy of the instrument within 0.05° in spectral range from $0.35\mu\text{m}$ to $0.8\mu\text{m}$, which was used in the contactless monitoring of thin non-homogeneous layers on the surfaces of metals and alloys.

The obtained digital images of corroded metal surfaces [5] allowing investigate their morphology and distribution of the corrosion film thickness over surface. It is also allows observing the corrosion changes under applied temperature, different chemical solutes and with time.

The digital images of a microscopic area of the alloy surface with a non-homogeneous nano-layer can be processed using modified to fit reflectometry an algorithm of spectroscopic imaging ellipsometry [8]. A tomographic approach to reconstructing the surface layers and films internal structure is proposed in [9]. As a source data for 3D structure, which is formed by solving an integral equation of the 1-st kind, is using the spectral ellipsometry measurements of light reflected from a non-uniform nano-layer surface.

Work [10] shows that digital optical images of coated metal surfaces, obtained with a typical scanner, allow measuring the

layer thickness at high accuracy (down to 1nm or even less) which is approved by the calculations, experiment, and by comparison with an independent ellipsometric method. As a test sample, the chrome steel alloy surface after a 1-h corrosion test from 100°C to 300°C temperature range was selected.

A combination of reflectometry based on PC optical scanner with diffuse reflection infrared spectroscopy (with a focused probing beam) [11] is an applicable for investigating the surface nonuniformity of the thermo-oxide layer thickness and chemical composition of oxide coatings on chromium steel and other alloys, which are affected by the oxidation in the air at a temperature of 500°C .

A combination of reflectometry based on PC optical scanner with electrochemical methods of controlling the pitting destruction is also possible [12]. It is allowing controlling the initial stages of the anodic dissolution of carbon steel under the influence of sodium chloride solution and exhibits noticeable formation of local defects looking as pits after only 1-hour tests.

Among existing software for visualization, processing and analyzing the reflectometry and ellipsometry data the Gwyddion [13] is most useful and dynamically developed solution. The main benefits are freeware, cross-platform, high scalable due to modular and plug-in paradigms, double precision native data format for operation and storage. Most of it modules are written in Python and 3D data display based on OpenGL.

Statistical analysis plug-ins include S_a , S_q , mean, median, range, skew, kurtosis, projected and surface area, entropy, inclination, which can be used for whole image or for areas under arbitrary masks. Also distributions and histograms creation using 1D and 2D angular distributions, 1D and 2D correlation functions, PSDF, Minkowski functional and other methods is performed.

Data correction uses: global and local outlier marking, scar marking, several line correction methods (median, modus), removal of data under arbitrary mask using Laplace or fractal interpolation, arbitrary polynomial deformation on xy -plane and more other. Also available software corrections for measurement instrumentation: correction of the scan axis drift and scale calibration, xy -plane rotation and affine distortion corrections. -Data processing methods includes: curve fitting, 1D- and 2D-FFTs, 2D-CWT, 2D-DWT, log-phi PSDF, wavelet anisotropy detection, and neural networks features.

Gwyddion developers investigated different [15] aspects of 3D scanning probe microscopy (SPM) and atomic force microscopy (AFM) instrumentation and related data evaluation algorithms, and proposed their solving:

- specialized software libraries written in C and LabVIEW for adaptive step (non-equidistant) SPM scanning techniques where individual x, y position data are recorded during measurements. Scanning with adaptive steps can reduce the amount of collected data [14];
- evaluation of nanoscale roughness of surfaces and their spectral properties using algorithms based on Fast Fourier Transform (FFT) not only for rectangular data but also for irregular and non-continuous data [17];
- setting of calibration error function for whole measurement volume, which allows determine the local values of uncertainty of the scanner and, in turn, converting them to yield local dimensional uncertainty values and use for evaluation of uncertainties related to the acquired data and for further data processing applications [18].

The presented article is devoted to a problem of developing software-based solution for visual plotting and numerical analyzing of thin film surfaces according to an experimental-obtained curve, which describes dependence between reflected wavelength and film thickness in nanometers.

I. THEORETICAL BACKGROUND

A. Structure of metal-oxide corrode film

A set of factors are significantly affected to the state of solid surfaces. Since the surface atoms of solids are relatively immobile, and in a greater degree their surface energy depends on the prehistory of the surface formation. For example, it is usually that the surface energy of a pure shatter of a crystal is lower than the energy of the polished surface of the crystal, and it is lower than the energy of the surface, which is subjected to heat treatment. A polishing is significantly effects on the properties of the surface. When it is applied a relatively deep fine-crystalline (pseudoamorphic) layer, which is resembling a film of a viscous liquid, is formed. This 'viscous liquid' flows into various roughness (cracks, scratches) [19].

The surface of different mechanisms is not perfectly smooth. Even after grinding on the surface of the metal, unevennesses of a height of one-hundredth or even one-tenth of the micrometer are preserved. Polishing also does not completely eliminate all roughness of surface of the metal.

The structure of the surface of polished metal region is schematically shown in Fig. 1. The oxide layer '1' is placed at the top. It should be note that oxide films with a thickness of $0.01\mu\text{m}$ to several millimeters are formed on a solid surface after contact with air (mixture of gases) for any duration (especially under high temperatures). They have different strength and adhesion to the surface of the metal, and in some cases well protect it from the corrode.

Underneath the oxide layer is the pseudoamorphous layer '2' which differs in properties from the other parts of the solid. It is more solid and more readily soluble in a liquid medium. It also carries a greater electrical charge. Below to the pseudoamorphous layer (sometimes called the Beilby layer) there is zone '3' called the deep deformation zone. Still lower is the region '4' called the large-scale deformation zone (thickness of $5-10\mu\text{m}$), and finally, there is the layer '5' of a weak deformation, which propagates to a depth of $20-50\mu\text{m}$.

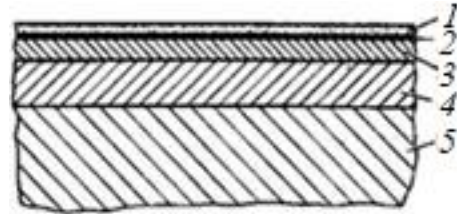


Fig. 1. Schematic structure of a polished metal surface.

The thickness of corrode films (oxide layers) formed on metals (it is usually referred to as d or h) varies within a wide range. The corrode films by criterion of their thickness are divided into three groups [20]:

- thin (invisible), which thickness is from fraction of nm to 40nm ;
- medium (giving the tint color), which thickness is within from 40nm to 500nm ;
- thick (visible), which thickness is more than 500nm and in many cases reaches a huge value (for example, a steel dross).

To determine the thickness d of films formed on metals or the specific amount of metal with oxide layer the different techniques are used. The research by Kostyakovsky, Evans, and Dankov [21] played an important role. The heat resistance of metals, and the laws of thickness growing of the metal films $d=f(\tau)$, mainly depends on the protective properties of the previously resulting films.

B. Obtaining the thickness of the corrode oxide layer

Let's consider the case of a numerical determination of the thickness of a layer and the refractive index of a transparent film, with known optical constants are n_s and k_s . Certainly, it was used equations for single-layer model with a substrate (Fig. 2).

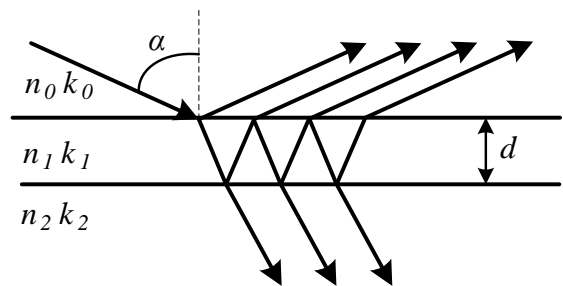


Fig. 2. Single-layer model with a substrate.

Ellipsometric parameters of a single-layer system were obtained [22, 23]:

$$tg\psi e^{i\Delta} = \frac{r_{a1p} + r_{10p}X}{1 + r_{a1p}r_{10p}X} \cdot \frac{1 + r_{a1s}r_{10s}X}{r_{a1s} + r_{10s}X}, \quad (1)$$

Where X is an exponential component:

$$X = e^{2\delta i}. \quad (2)$$

Argument of this expression is named phase layer thickness:

$$\delta = 2\pi \frac{d}{\lambda} \sqrt{n_1^2 - \sin^2(\alpha)}. \quad (3)$$

The thickness of layer can be derived by using the Holmes method.

C. Converting RGB-palette color to wavelength

Any existing scanner returns result to any digital device with image view. As a rule, the image is a set of pixels in the RGB color space. Next going to the wavelength of the falling ray of light based on the resulting set of RGB values of one pixel is not a simple task. There are many color spaces, which are used in different applications. Moreover, there are color areas, which couple with wavelengths. For example, it is XYZ color space.

Converting from RGB to XYZ model can be calculated by the following formula:

$$\begin{bmatrix} X \\ Y \\ Z \end{bmatrix} = \begin{bmatrix} m_{11} & m_{12} & m_{13} \\ m_{21} & m_{22} & m_{23} \\ m_{31} & m_{32} & m_{33} \end{bmatrix} \cdot \begin{bmatrix} R \\ G \\ B \end{bmatrix}, \quad (4)$$

where are $m_{11} \dots m_{33}$ – coefficients of converting matrix, XYZ – coordinates of CIE 1931 color space, RGB – color part of RGB color model. If we cut section from XYZ model, while there is a condition:

$$X + Y + Z = const, \quad (5)$$

the linearly independent coordinates can be obtained in the form:

$$x = X / (X + Y + Z), \quad y = Y / (X + Y + Z). \quad (6)$$

The color chromatic diagram with wavelengths of colors is shown in Fig.3, and based on it, the dependence of the wavelength on values of coordinates x and y can be derived.

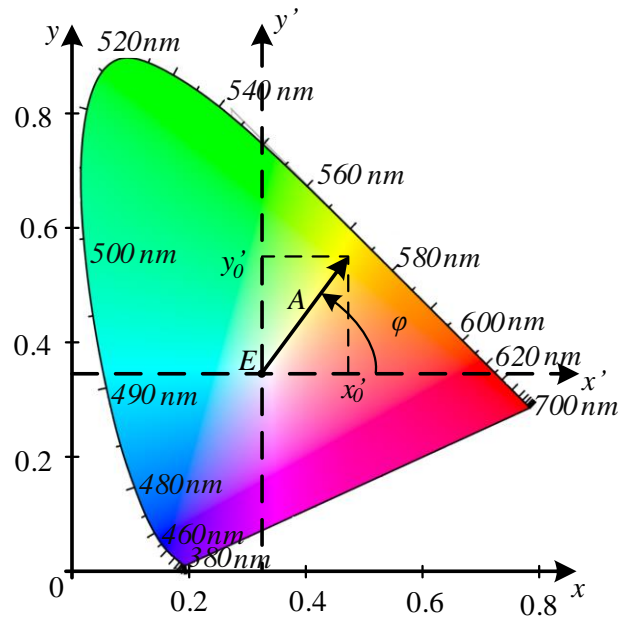


Fig. 3. Chromatic diagram with wavelengths of colors.

The method of getting the dependence is a creating additional coordinate system with axes are x' and y' . The center of this system of axes is a point $E(0.33, 0.33)$, which corresponds to the "Equal Energy" white color. For obtaining wavelength's values, the coordinates x' and y' were taken as coordinates of vector A. The rotation angle with respect to the positive direction of the x' axis sets the color tone. Length of this vector determines saturation value, but it is not taken into account.

So, the task is to get angle of rotation of system with axis x' and y' , with condition is that RGB values are the input parameters.

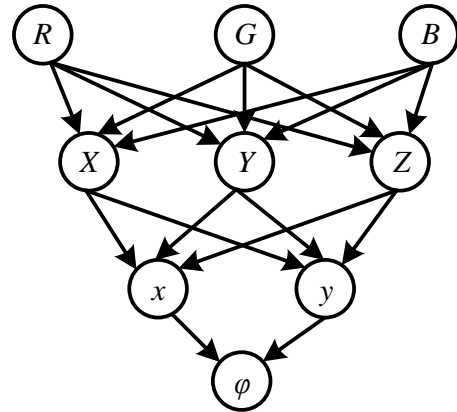


Fig. 4. Tree of finding angle of rotation.

Fig.4 shows the angle of rotation finding tree. The finding of angle can be solved with using math function is arctangent. It is like getting argument of complex number.

The resulting dependence is shown in Fig. 5 (a), but this statement does not coincide with practice. Thus, it was proposed the dependence in Fig. 5 (b) for use, which is different with the first one at range of violet part.

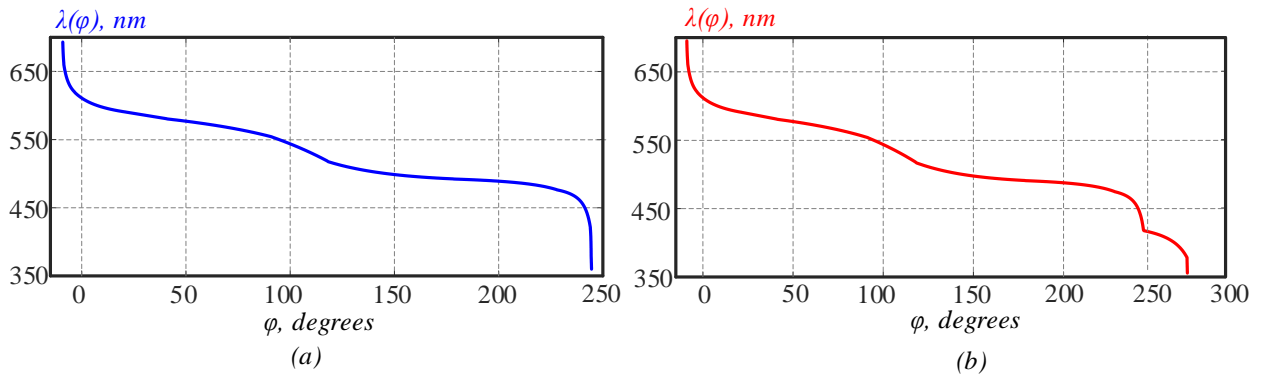


Fig. 5. The dependence of the thickness of layer on angle of rotation in $x'y'$ system: Theoretical statement (a), Experimental statement (b).

D. Selection the types of light source and sensor of reflected light

A four mainly used light sources types in PC-scanners exist. Let's compare them by the quality of spectral irradiation characteristic and the light stability.

Luminescent lamp with a hot cathode. Has the best efficiency and the most linear and smooth spectral irradiation characteristic, which additionally can be controlled and low start-up time around a few second. The disadvantages are degradation with time, and, thus, the time instability, low life cycle around 1000 hours, and continuous on-mode during the scanning process.

Luminescent lamp with a cold cathode. Such type of lamps has a long service life (up to 10000 hours), low operational temperature, linear and smooth spectral irradiation characteristic, which might be worsened, when the light intensity is increased. Among the disadvantages, the longest start-up time (up to few minutes) and the highest power consumption are existing.

Light-Emission diode (LED). They are usually uses in CIS-scanners. Among their advantages are the low power consumption, near to zero the start-up time and the smallest size among all types of light source. In most cases the RGB LED is continuously changes its color wavelength during scanning. Nevertheless, they has low light intensity, and the worst disadvantage is in limited and non-linear irradiation spectrum, which is dramatically worsen the scanning characteristics in our case.

That is why, as a light-source device, a mercury-free xenon (Xe) gas discharge lamp with a cold cathode and the internal fluorescent phosphor (P) coating is used [24], which has many advantages:

- spectral irradiation characteristic that is more linear and smooth in visible range than mercury ones;
- spectral irradiation emission spikes are presented only in the infrared (above the 800nm wavelength);
- near to zero start-up time due to the absence of cathode preheating;
- small size and long life cycle.

Nevertheless, they have low light intensity, low energy efficiency and high supply voltage (up to 2kV).

In PC-scanners a two types of photometric sensors are mainly use: Charge Couple Device (CCD) and Contact Image Sensor (CIS). The second type of sensors has a truncated optical subsystem (mirror, prism and objective-glass are absent) and, therefore, has worse resolution, sensitivity and depth of field.

The CCD cells have different sensitivity, i.e. even under the absolutely homogenous illumination, the are gives different output signal (sometimes called geometric noise). The value of this heterogeneity does not exceeds 2-5% (for different quality of producing). In system, where the high photometric precision is a significant factor, it can be simply eliminated by using of preliminary calibration under at least two illumination intensities and store of the CCD output data into lookup-table. This data are used as a calibration coefficients in all subsequent measurements, but only after performing the correction of the dark noise.

II. SOFTWARE SOLUTION DESCRIPTION

The software solution is written in C++ using Qt Creator SDK, and consists of two windows, these are main window and graph's window (Fig. 6). In its turn, the main window consists of the next blocks:

- the input picture block, which includes itself ability to loading a picture into program and showing image in the window;
- the graph list allows to choose the graph, which is needed to use by user for drawing of 3D picture;
- 3D picture shows result of getting corrode oxide layer thickness. This block based on OpenGL.

Beside these blocks the user can move to graph window by double click on list box "Change graphs". This window has different block, but the main aim is operation with points of diagram. The opportunities of graph window are the next:

- manually moving points in the diagram.
- add coordinates of new point.
- creating new graph, and save it to graph list.
- change the range and scope area of the axes.
- change coordinates of existing point.
- saving and restoring diagram.

Axis x corresponds to values of wavelength, and axis y is layer thickness. After setting the necessary dependence in diagram, the user can see the refreshed 3D for current picture, which was previously uploaded. View of this block can rotate by mouse. And there is the normal view button to return in eye-catching view. The user can set different experimentally-obtained dependences to clarify three-dimensional model for a sample of alloy by using of developed software.

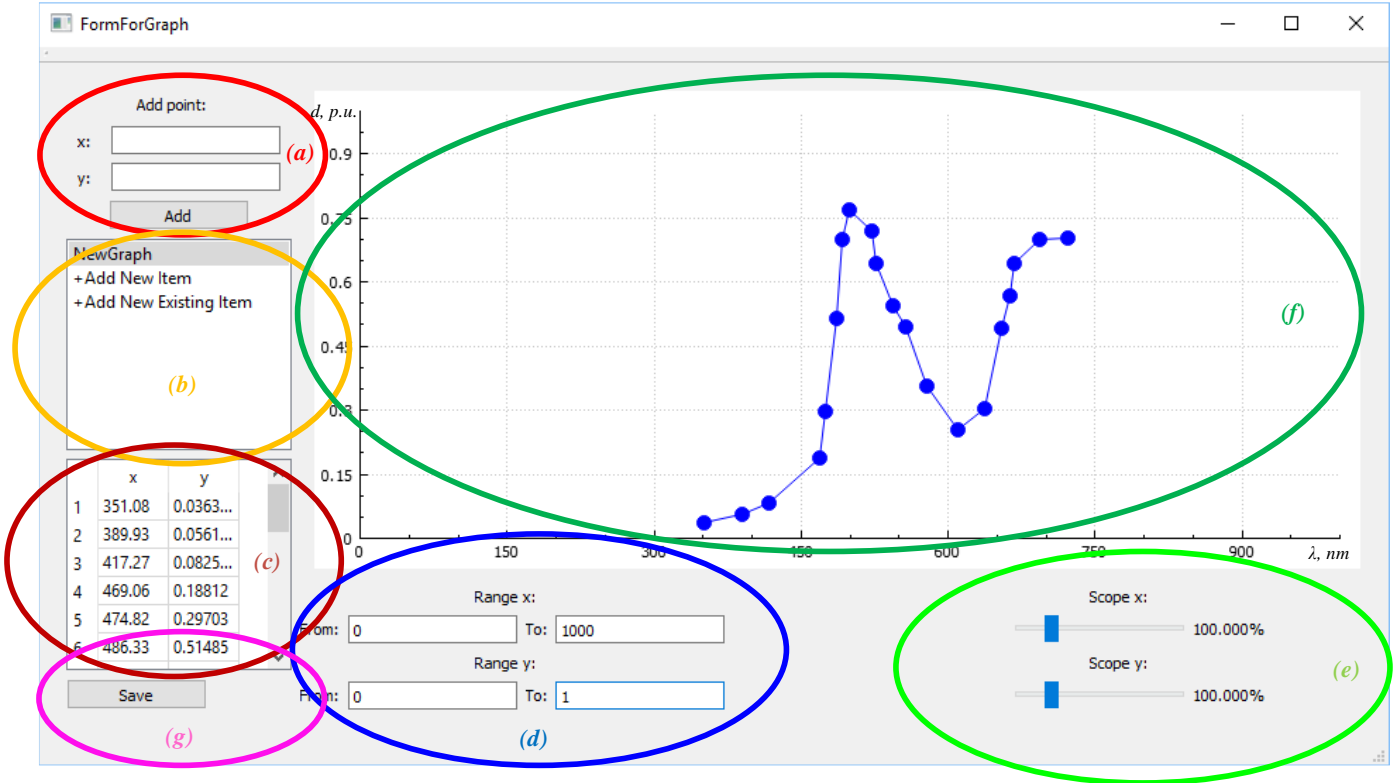


Fig. 6. Graph's window: block of adding a new point (a), list of graphs with possibility to read existing diagram from file (b), table of the existing points in current graph (c), block of changing axes range (d), block of scope axes (e), canvas of wavelength-thickness curve (f), block of saving the points of current graph (g).

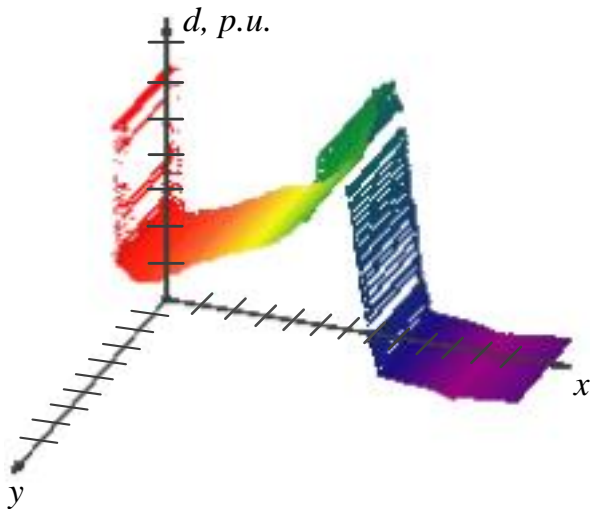


Fig. 7. Result of building 3D model based on wavelength-thickness curve setting-up in Fig.6 (f).

III. EXPERIMENTAL RESULTS

For converting from RGB model to XYZ-area, the coefficients of the CIE RGB space were taking in calculation. The matrix coefficients are used in the next equation:

$$\begin{bmatrix} X \\ Y \\ Z \end{bmatrix} = \begin{bmatrix} 0.4887180 & 0.3106803 & 0.2006017 \\ 0.1762044 & 0.8129847 & 0.0108109 \\ 0.0000000 & 0.0102048 & 0.9897952 \end{bmatrix} \cdot \begin{bmatrix} R \\ G \\ B \end{bmatrix}. \quad (7)$$

Table I shows the theoretical and experimental results of converting RGB values to wavelength for different colors.

TABLE I. WAVELENGTH AND RGB VALUES FOR DIFFERENT COLORS.

Color	Range of Lengths waves, nm	RGB			Wavelength Result, nm
		Red	Green	Blue	
Violet	≤450	90	0	157	417.232
Blue	450 – 480	0	77	255	472.77
Blue-green	480 – 510	0	255	255	493.584
Green	480 – 550	0	255	0	545.213
Yellow-green	550 – 570	154	205	50	564.387
Yellow	570 – 590	255	255	0	570.526
Orange	590 – 630	255	83	0	590.349
Red	≥630	255	0	0	700

For verification of previously proposed technique, a test profile diagram was manually set (it is shown in Fig. 6(f)), and it caused to build corresponding 3D model, as it is presented in Fig.7.

CONCLUSION

The methods of reflectometry and ellipsometry for metal and alloy corrode film topology and thickness investigation using customer digital scanners and cameras were examined. A software-based solution, implemented in C++ with Qt Creator SDK for visual plotting and numerical analyzing of corrode surfaces, according to an experimental-obtained dependence between reflected wavelength and oxide film thickness in nanometers, was implemented and tested with existing experimental data. Developed application allows managing previously measured curves for different alloys at different temperature range by manual editing of curve vertices, on-line replot of the 3D surface and measure averaged thickness, minimal and maximal values, and deviation. An engineering clarification of chromatic color diagram in violet range, which allowing correlate violet tones with correct wavelengths, was performed. Developed application can be also used for monitoring of inhibitors adsorption at steel [25].

REFERENCES

- [1] V.A. Kotenev, M.A. Petrunin, L.B. Maksaeva, and A.Y. Tsivadze, "3D visualization of the dissolution products of a metal in the near-electrode layer at the metal-solution interface," *Protection of metals*, 41(6), pp.507-520. November 2005.
- [2] V.A. Kotenev, "A digital microreflectometrical video 3D-probe for the corrosion studies," *Protection of metals*, 38(4), pp.382-391. July 2002.
- [3] V.A. Kotenev, "Automation of Hand-Operated Ellipsometers," *Instruments and Experimental Techniques*, 45(6), pp.801-805. November 2002.
- [4] V.A. Kotenev, "Computer scanners as a means of monitoring corroded surfaces. The thickness and topography of corrosion layers," *Protection of Metals*, 37(3), pp.254-261. May 2001.
- [5] V.A. Kotenev, "Digital polarizing 3D microscopy for monitoring the quality of electroplates," *Protection of metals*, 38(6), pp.595-601. November 2002.
- [6] V.A. Kotenev, "Digital-Reflectometry Characterization of the Surface Structure and Protective Property of Thin Films," *Russian Microelectronics*, 31(6), pp.396-406. November 2002.
- [7] V.A. Kotenev, "Information-optical 3D-techniques for corrosion monitoring," *Protection of metals*, 40(5), pp.407-420. September 2004.
- [8] V.A. Kotenev, and A.Y. Tsivadze, "Microspectroscopic imaging of heterophase layers of metal-oxide sensors using a video camera," *Russian Journal of Inorganic Chemistry*, 52(4), pp.567-576. April 2007.
- [9] V.A. Kotenev, "Nanotomography: Ellipsometric Spectral Tomography of Surface Nanostructures Metal-Oxide," *Protection of metals*, 39(4), pp.394-404. July 2003.
- [10] V.A. Kotenev, "Potentialities of computer scanners in monitoring hyperthin layers," *Protection of metals*, 40(4), pp.394-401. July 2004.
- [11] V.A. Kotenev, N.P. Sokolova, and A.M. Gorbunov, "Scanner 3D-probe and infrared probe spectroscopy for investigating macrodefects of thermooxide layers," *Protection of metals*, 38(5), pp.424-430. September 2002.
- [12] M.A. Petrunin, L.B. Maksaeva, D.N. Tyurin, and V.A. Kotenev, "Scanning electrochemical diagnostics of initial stages of anodic dissolution of carbon steel in chloride containing solutions," *Protection of Metals*, 44(5), pp.529-532. September 2008.
- [13] D. Nečas, and P. Klapetek, "Gwyddion: an open-source software for SPM data analysis," *Open Physics*, 10(1), pp.181-188. February 2012.
- [14] P. Klapetek, A. Yacoot, P. Grollich, M. Valtr, and D. Nečas, "Gwyscan: a library to support non-equidistant scanning probe microscope measurements," *Measurement Science and Technology*, 28(3), p.034015. January 2017.
- [15] D. Nečas, and P. Klapetek, "Study of user influence in routine SPM data processing," *Measurement Science and Technology*, 28(3), p.034014. January 2017.
- [16] P. Klapetek, and D. Nečas, "Independent analysis of mechanical data from atomic force microscopy," *Measurement Science and Technology*, 25(4), p.044009. March 2014.
- [17] D. Nečas, and P. Klapetek, "One-dimensional autocorrelation and power spectrum density functions of irregular regions," *Ultramicroscopy*, 124, pp.13-19. January 2013.
- [18] P. Klapetek, D. Nečas, A. Campellová, A. Yacoot, and L. Koenders, "Methods for determining and processing 3D errors and uncertainties for AFM data analysis," *Measurement Science and Technology*, 22(2), p.025501. January 2011.
- [19] A.A. Bratkov, "Theoretical Principles of Chemmotology," [in Russian] Khimiya, Moscow, 1985.
- [20] N. P. Zhuk, "A Course of the Theory of Corrosion and Protection of Metals," [in Russian] Metallurgiya, Moscow, 1976.
- [21] P.D. Dankov, "Laws of the Formation and Structure of Protective Films on Metals," In *Proc.(Doklady) Acad. Sci. USSR*, vol. 23, p. 548, 1939.
- [22] M. Born, and E. Wolf, "Principles of optics: electromagnetic theory of propagation, interference and diffraction of light." Elsevier, 2013.
- [23] V.V. Scorcelletti, "Theoretical Fundamentals of Corrosion in Metals," *Khimiya, Leningrad*, 1973.
- [24] H., Noguchi, and H. Yano, "37.2: A Mercury-Free Cold Cathode Fluorescent Lamp for LCD Backlighting," In *SID Symposium Digest of Technical Papers*, vol. 31, no. 1, pp. 935-937). Blackwell Publishing Ltd, May 2000.
- [25] O.I. Sizaya, O.N. Savchenko, A.A. Korolev, and V.G. Ushakov, "Adsorption of Inhibitors Based on Vegetable Raw Materials at Steel," *Protection of Metals*, Vol. 44, No. 3, pp. 248–252. May 2008.